Self-assembly of Fine Particles Applied to the Production of Antireflective Surfaces

Hayato Kobayashi[1], Nobuyuki Moronuki[1,#] and Arata Kaneko[1]

1Graduate school of System Design, Tokyo Metropolitan University, 6-6, Asahigaoka, Hino, Tokyo, Japan, 191-0065
#Corresponding Author / E-mail: moronuki@tmu.ac.jp, TEL: +81-42-585-8606, FAX: +81-42-583-5119

KEYWORDS: Structured surface, Self-assemble, Fine particles, Antireflection

We introduce a new fabrication process for antireflective structured surfaces. A 4-inch silicon wafer was dipped in a suspension of 300-nm-diameter silica particles dispersed in a toluene solution. When the wafer was drawn out of the suspension, a hexagonally packed monolayer structure of particles self-assembled on almost the complete wafer surface. Due to the simple process, this could be applied to micro- and nano-patterning. The self-assembled silica particles worked as a mask for the subsequent reactive ion etching. An array of nanometer-sized pits could be fabricated since the regions that correspond to the small gaps between particles were selectively etched off. As etching progressed, the pits became deeper and combined with neighboring pits due to side-etching to produce an array of cone-like structures. We investigated the effect of etching conditions on antireflection properties, and the optimum shape was a nano-cone with height and spacing of 500 nm and 300 nm, respectively. This nano-structured surface was prepared on a 30 × 10-mm area. The reflectivity of the surface was reduced 97% for wavelengths in the range 400–700 nm.

Manuscript received: October 18, 2007 / Accepted: December 12, 2007

1. Introduction

Low-reflectivity surfaces are required in various products such as solar panels and flat panel displays[1], and a regular surface structure with a spacing shorter than the wavelength of incident light exhibits antireflective behavior.

Several processes have been proposed for fabricating low-reflectivity structures. A typical one is the combination of electron beam (EB) lithography and a dry etching process such as reactive ion etching (RIE)[2,5]. Kanamori et al. fabricated an antireflective surface with a conical shape structure 350 nm in height and 150 nm in pitch using EB lithography and the fast atom beam (FAB) process, which is one of the dry etching processes[6]. Its reflectivity decreased from 54.7% to less than 0.5% for a wavelength of 400 nm. Although EB lithography does permit fine patterning, it is not suitable for large areas over a square centimeter, for example, because of the time it requires. Therefore, a new method of nano-patterning is needed for creating antireflective surfaces on large areas.

We focused on the self-assembly of particles using the dip-coating method[7-8] to overcome this limitation. The process is very simple. The substrate is dipped into suspension that contains dispersed nanoparticles and then drawn out of the suspension at a constant speed. This process readily permits the self-assembly of particles with a hexagonally close-packed structure. One of the applications of self-assembled particles is masks for patterning in dry etching[9,10] and deposition[11,14]. Fine patterning with various spacings is possible by changing the diameter of the particle. Some research has investigated the application of self-assembled particles as masks to produce antireflective surfaces[15].

The dip-coating process has other advantages such as scalability and low cost. Meter-size assembly would be possible without any complex setup, while the scalability of EB lithography is limited due to the necessity of a vacuum environment. However, assembly tends to randomness while EB lithography assures perfect regularity. Thus, examining the effect of this randomness on optical properties is necessary to understand the total process.

In this paper, we propose and demonstrate the combination of dip-coating and RIE to create large-area antireflective surfaces.

2. Principle

Light is reflected at the interface of two objects with different refractive indices, and Fig. 1 presents the principle of an antireflective surface with a nanostructure assuming incident light from air to glass. The upper illustration of Fig. 1(a) shows the behavior of the light incident on a flat surface. In this case, the light reflects at the boundary. The lower illustration in Fig. 1(a) shows the spatial distribution of the refractive index. The refractive index of air is 1, and that of glass is about 1.4. The refractive index changes discontinuously from 1 to 1.4 at the boundary and reflects the light. Figure 1(b) presents the principle of the antireflective effect caused by a structured surface. The upper illustration in Fig. 1(b) indicates the behavior of the light incident on the structured surface. The structure is assumed to be an array of conical shapes with a period shorter than the wavelength of the light. The lower illustration in Fig. 1(b) shows the distribution of the refractive index. With the nanostructure, the refractive index at the boundary changes continuously. The effect of the structure on the light can be neglected because the structure is smaller than its wavelength, and the refractive index at the structured surface can be treated as the intermediate value between that of glass

and air. The local density of glass increases continuously from that of air to the glass side, then the refractive index changes from 1 to 1.4 continuously. Thus, light reflection can be prevented.

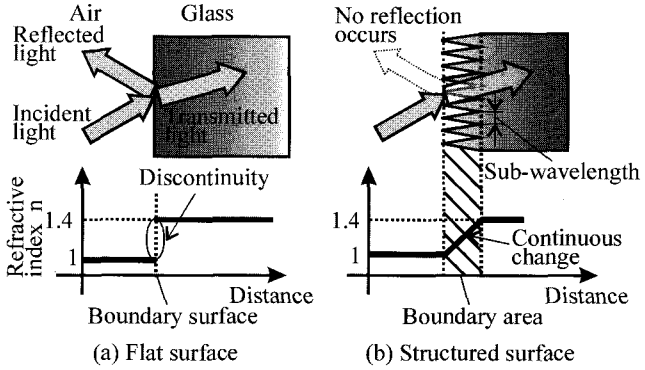

Fig. 1 Principle of the antireflective effect caused by a structured surface

3. Experiments

3.1 Setup and self-assembly of particles

Figure 2 presents the experimental setup for self-assembly of particles together with its underlying principle. Figure 2(a) shows the schematic of the setup. A reservoir was filled with a suspension containing nanoparticles. The substrate was dipped into the suspension and then drawn out at constant speed by a motorized stage. Figure 2(b) is a close-up of the cross section A–A' showing the interface between the substrate, the suspension, and the air. The surface tension attracts the suspension, and local flow along the substrate is generated by the combination of the natural evaporation of the solvent and the upward motion of the substrate. Particles move with the flow and aggregate on the substrate. At the final stage of assembly, the particles attract each other due to the meniscus force to form a close-packed structure. The conditions such as the drawing speed and the concentration affect the results to determine the surface coverage and whether a monolayer is formed.

The top view of self-assembled particles is shown in Fig. 2(c). Ideally, particles on the substrate form a close-packed structure as described above, and openings exist between the particles. By using the particles as a mask, we etched through these openings. The conditions we used are as follows. The particles were SiO_2, 300 nm in diameter, and the suspension concentration was 5 wt%. The solvent was toluene that contained approximately 1% acrylic resin as a dispersant as well as a binder to fix the particles to the substrate. This suspension is commercially available. The substrate was a 4-inch Si wafer ultrasonically cleaned with ethanol and purified water before the experiments. The drawing speed was 560 μm/s.

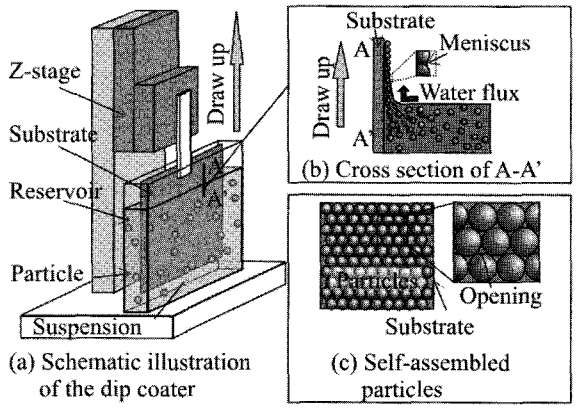

Fig. 2 Schematic diagram of the self-assembled particle process

3.2 Etching process

Figure 3 presents a schematic of the RIE process. Figure 3(a) shows the cross section of self-assembled particles on the substrate. Figure 3(b) illustrates an early stage of etching. Openings between particles are etched off selectively, and pits form on the substrate. Figure 3(c) shows the principle for fabricating the tapered shape. RIE combines two different etching processes; one is anisotropic or physical etching and the other is isotropic or chemical etching. The anisotropic process etches mainly in the direction of ion bombardment and hardly touches the sidewalls. In contrast, the isotropic process etches in all directions. Thus, the sidewalls of the pits are etched beneath the masks and is called side-etching. The etching conditions such as electric power and pressure determine the balance of these two etching processes and thus the tapered profile. After etching, the remaining particles were removed by ultrasonic cleaning with toluene. Figure 3(d) shows the final profile. The RIE equipment was the parallel plate type (Samco International Inc., BP-1).

Figure 4 presents the system for measuring the reflectance. The light with an adjustable wavelength in the range 400–700 nm was produced by a monochoromator. The incident light was projected on the sample over the area of ϕ1 mm. The intensity of the reflected light was detected by a photomultiplier and its intensity was sent to a personal computer (PC). The incident and reflection (detection) angles were fixed at 30° in this experiment. It is generally difficult to quantify the absolute reflectance because the power spectrum of the light source must be calibrated. Thus, in this study, we discuss relative reflectance, which is the ratio of the reflective intensity of the sample to that of the original mirror-finished substrate.

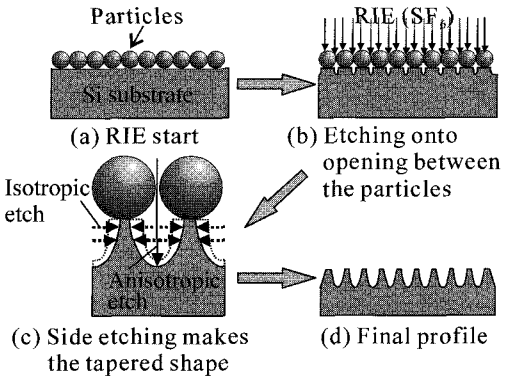

Fig. 3 Schematic of the RIE process flow

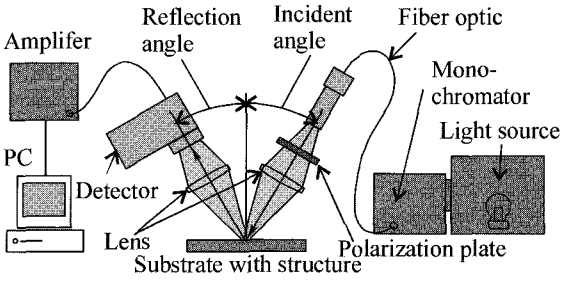

Fig. 4 Measurement system for light reflectance

4. Results and Discussion

4.1 Self-assembly of particles

Figure 5 shows the scanning electron microscopy (SEM) images of the self-assembled particles. Figure 5(a) illustrates the case in which the wafer was drawn up once. Particles assembled, leaving some vacancies, and the coverage of particles on the substrate was calculated to be 70% by analyzing the image. The coverage of a perfectly close-packed structure is about 85% and is thus the upper limit. Vacant areas do not work as mask, and so no structure will be fabricated on such areas. Particles on the substrate were fixed to the

substrate with the binder contained in the suspension and did not peel off during repeated dip-coatings. Figure 5(b) shows the result of dip-coating twice. The coverage increased up to 80% although vacancies still present. Figure 5(c) shows the result after dip-coating three times. The coverage increased up to 85% though line defects were present instead of vacancies. The effect of line defects on the final shape may be neglected because the size of the defect was about 100 nm and is comparable with the spacing of the structure.

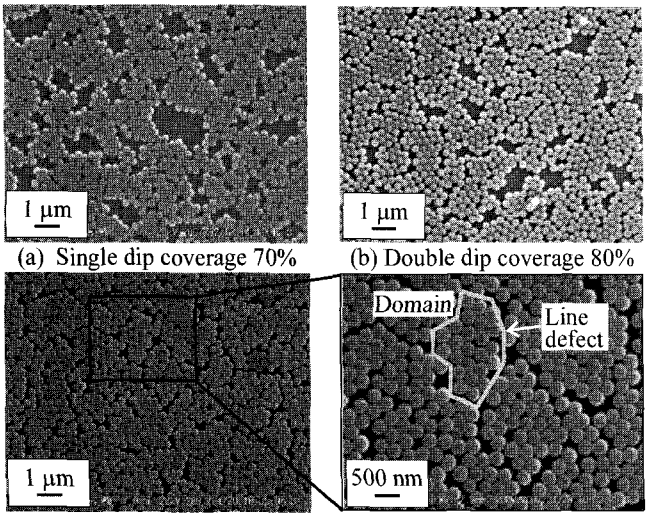

Fig. 5 Comparison of substrate dip-coated different numbers of times

Figure 6 shows the entire substrate and SEM images of different points on it after triple dip-coating. We found that particles assembled in a monolayer all over the wafer although defects were distributed across the entire surface. This process can be applied to larger substrates because of this simple principle. We have shown that the experimental conditions were appropriate for fabricating a monolayer array of particles for a large area.

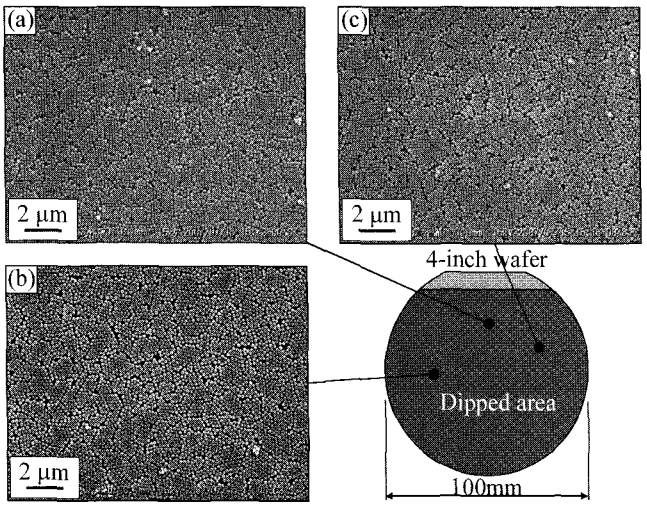

Fig. 6 Image of the entire substrate and self-assembled particles at each observed point

The coverage was improved by repeating the dip-coating process. In subsequent dip-coatings, the suspension probably gathered and was trapped only in the vacancies or hollow parts, and then the particles assembled there. Note that no multilayer structures were observed. The wettability of the first layer of particles was different from that of the Si substrate because of acrylic binder, and this prevented another particle being assembled under the same drawing conditions. Thus, it enabled improved coverage while maintaining the monolayered structure.

Usually, the structure would change from a monolayer to multilayers with the increase in coverage. However, the monolayer condition is difficult to predict because the dip-coating process is strongly affected by conditions such as wettability. In this case, the surface wettablity could change after the first dip-coat because the substrate was covered by an acrylic layer. Thus, it would seem that particles would be difficult to assemble on the substrate. However, the reason for this result is not clear from our experiments, and further investigation is required.

4.2 Surface structure and reflectance

The substrates were etched using RIE, and the effect of vacancies on the structural shape and the reflectance was investigated. The substrates had different coverages, 70, 80, and 85%. The RIE conditions are shown in Table 1. These conditions were determined through preliminary experiments.

Table 1 RIE conditions

Etching gas	SF_6
Electric power (W)	10
Vacuum (Pa)	6.67
Time (s)	300

Figure 7 shows the SEM images of the substrate after RIE. Figure 7(a) presents the case of 70% coverage before ultrasonic cleaning. We confirmed that particles remained after etching and functioned as a mask. The openings between the particles were etched off and vacant areas were etched flat. Figure 7(b) shows the image of the substrate after ultrasonic cleaning. The particles were removed to reveal the structured surface. The shape of the structure was almost conical with height ranging from 200 to 500 nm and the period was the same as the 300-nm particle diameter. Figures 7(c) and (d) show the images of the etched substrates with 80 and 85% coverage, respectively. The flat areas decreased with an increase in coverage. The shape of the structure is the same as that for 70% coverage.

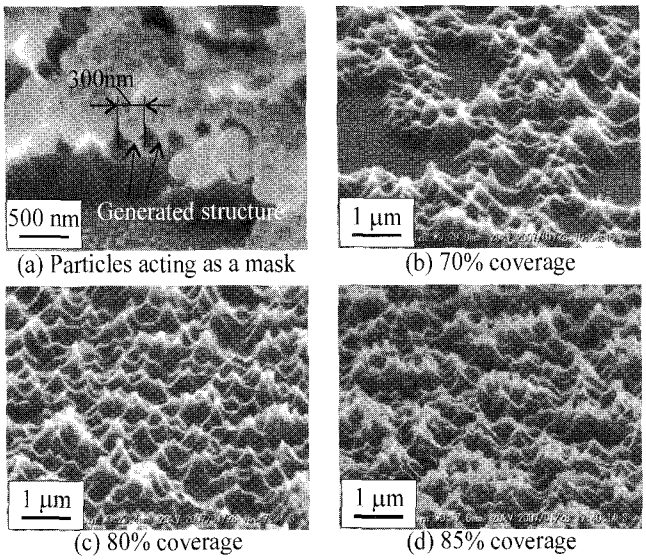

Fig. 7 SEM images of the structured surface with different particle coverage

Figure 8 shows the relative reflectance of the substrates with different coverages. The projected beam spot size was about ϕ1 mm as noted above. The horizontal axis denotes the wavelength of theincident light and the vertical axis is the relative reflectance. The relative reflectance decreased to less than 10% in all cases. In the case of the 80 and 85% coverage, the reflectance decreased to 3% for a wavelength of 400 nm. Higher coverage of particles and structure clearly results in better antireflection properties.

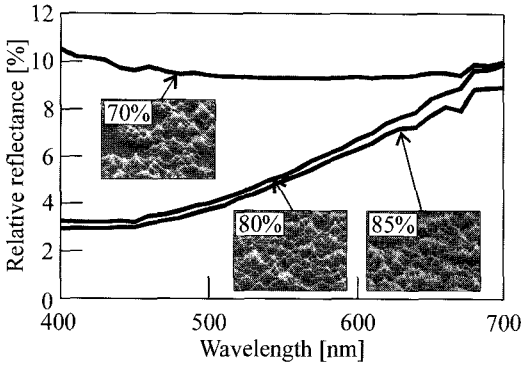

Fig. 8 Comparison of reflectance for samples with different coverages

Next, to investigate the effect of the structural shape, we examined the effect of the etching time. We etched dip-coated substrates with 85% coverage for different times, 120, 300, and 420 s. The other RIE conditions are shown in Table 2.

Table 2 RIE conditions

Etching gas	SF_6
Electric power (W)	10
Vacuum (Pa)	6.67
Time (s)	120, 300, 420

Figure 9 illustrates the effect of etching time on the structure shape. Figure 9(a) shows the case of 120 s. The substrate was not sufficiently etched and flat surfaces remained over large areas. Figure 9(b) shows the case of 300 s. As etching progressed, conical-shaped structures with the period of the mask particles became clear. The height and period of the structure were approximately 500 nm and 300 nm respectively, which is the preferred shape for antireflective surfaces. Figure 9(c) shows the case of 420 s. The conical shape has disappeared because of excess side etching. The side etching that had formed the conical shape etched it away it as shown in Fig. 9(d). Thus, 300 s was the appropriate etching time under these conditions.

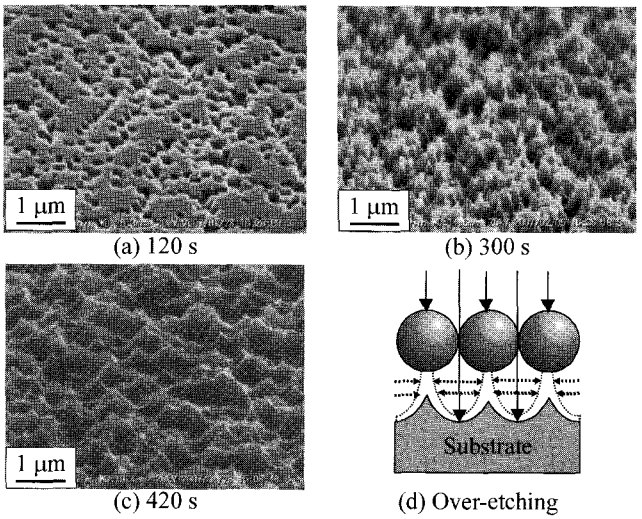

Fig. 9 SEM images of the structured surface with different etching times

Figure 10 shows the relative reflectance of samples with different etching times. The case of 120 s showed the highest reflectance because flat surfaces remained. The case of 300 s etching had the lowest reflectance, less than 3% for wavelengths in the range 400–700 nm, indicating that this was a suitable method for producing antireflective structured surfaces. The reflectance of substrates etched 420 s increased to 4%.

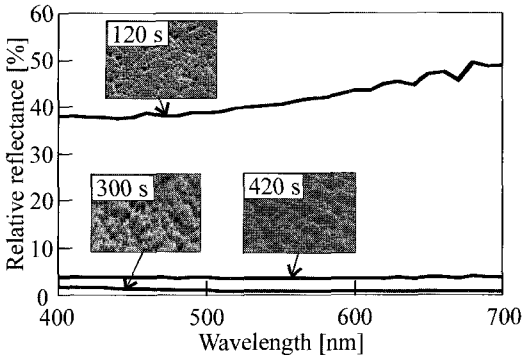

Fig. 10 Comparison of reflectance among samples with different etching times

Figure 11(a) is a photograph of the original mirror-finish substrate before processing beside the etched version. The camera that took this photograph can be seen in the picture due to the good reflection in the unprocessed substrate. The processed substrate appears black because of its low reflectivity. This confirms that the processed substrate has antireflection properties. Figure 11(b) shows the close-up SEM image of the processed substrate. The spacing between the structures corresponds to the 300-nm diameter of the particles. Flat areas can be observed at the tips of the cones. This tends to reduce the reflectivity a little more. The randomness of the assembly seems preferable because it prevents the diffraction or interference of the light. Other experiments are necessary to verify this.

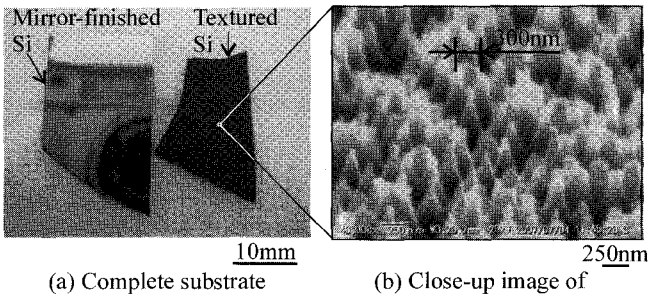

(a) Complete substrate (b) Close-up image of the textured surface

Fig. 11 Typical example of a Si substrate with textured surface

5. Conclusions

We have demonstrated a process for producing antireflection surfaces. The results are summarized as follows.

1) Particles 300 nm in diameter made of SiO_2 were self-assembled on 4-inch Si wafers (7000 mm^2) with a coverage of 85%.
2) By using the particles as a mask for RIE, nano-cone arrays were fabricated 500 nm in height and 300 nm in pitch.
3) The relative reflectance of the processed surface decreased to less than 3% that of the unprocessed mirror-finished Si wafer.

The replicating or imprinting process should be taken into account when considering the mass production of these nano-sized features. Further scale extension poses another challenge.

REFERENCES

1. Song, J. Y., Park, H. Y., Kim, H. J. and Jung. Y. W., "Development of Defect Inspection System for PDP ITO Patterned Glass," International Journal of Precision Engineering and Manufacturing, Vol. 7, No.3, pp. 18–23, 2006

2. Toyoda, H., Takahara, K., Okano, M., Yotsuya, T. and Kikuta, H., "Fabrication of microcone array for antireflection structured surface using metal doted pattern," Japanese Journal of Applied

Physics, Vol. 40, No. 7B, pp. 747–749, 2001.

3. Kanamori. Y., Kikuta, H. and Hane, K., "Broadband antireflection gratings for glass substrates fabricated by fast beam etching," Japanese Journal of Applied Physics, Vol. 39, No. 7B, pp. 735–737, 2000.

4. Zhou, J., Yang, G., "Nanohole Fabrication using FIB, EB and AFM for Biomedical Applications," International Journal of Precision Engineering and Manufacturing, Vol. 7, No. 4, pp. 18–22, 2006.

5. Lee, G. I., Kim, K., Jeon, S. C., Kim, J. S. and Lee, H. M., "Nanophotonics of Hexagonal Lattice GaN Crystals Fabricated using an Electron Beam Nanolithography Process," International Journal of Precision Engineering and Manufacturing, Vol. 7, No. 4, pp. 14–17, 2006.

6. Kanamori, Y., Sasaki, M. and Hane, K., "Broadband antireflection gratings fabricated upon silicon substrates," Optics Letters, Vol. 24, No. 20, pp. 1422–1424, 1999.

7. Denkov, N. D., Velev, O. D., Kralchevsky, P. A., Ivanov, I. B., Yoshimura, H. and Nagayama, K., "Two-dimensional crystallization," Nature, Vol. 361, No. 6407, p. 26, 1993.

8. Kaneko, A., Moronuki, N., Mogi, M. and Yamamura, Y., "Fabrication of self-assembled microstrcuture on using controlled liquid spreading on textured surface," Proceedings of the 11th International Conference on Precision Engineering, pp. 191–196, 2006.

9. Han, S., Hao, Zhibiao., Wang, J. and Luo, Y., "Controllable two dimensional photonic crystal patterns fabricated by nanosphere lithography," Journal of Vacuum Science and Technology, Vol. 23, No. 4, pp. 1585–1588, 2005.

10. Cheung, C. L., Nikolic, R. J., Reinhardt, C. E. and Wang, T. F., "Fabrication of nanopillars by nanosphere lithography," Nanotechnology, Vol. 17, Issue 5, pp. 1339–1343, 2006.

11. Hulteen, J. C., Treichel, D., Smith, M., Duval, M.., Jensen, T. and Duyne, R., "Nanosphere lithography: Size-tunable silver nanoparticle and surface cluster arrays," Journal of Physical Chemistry B, Vol. 103, Issue 19, pp. 3854–3863, 1999.

12. Wellner, A., Preece, P. R., Fowler, J. C. and Palmer, R. E., "Fabrication of ordered arrays of silicon nanopillars in silicon-on-insulator wafers," Microelectronic Engineering, Vol. 57–58, pp. 919–924, 2001.

13. Astilean, S., "Fabrication of periodic metallic nanostructures by using nanosphere lithography," Romanian Reports in Physics, Vol. 56, No. 3, pp. 340–345, 2004.

14. Cheng, S. L., Lu, S. W., Li, C. H., Chang, Y. C., Huang, C. K., and Chen, H., "Fabrication of periodic nickel silicide nanodot arrays using nanosphere lithography," Thin Solid Films, Vol. 494, Issue 1-2, pp. 307–310, 2006

15. Nakanishi, T., Hiraoka, T., Fujimoto, A., Saito, S. and Asakawa, K., "Nano-patterning using an embedded particle monolayer as an etch mask," Microelectronic Engineering, Vol. 83, Issue 4–9, pp. 1503–1508, 2006.